Nematic order director fluctuations in cylindrical capillaries

P. Ziherl and S. Žumer
Department of Physics, University of Ljubljana, Jadranska 19, 1000 Ljubljana, Slovenia
(Received 7 March 1996)

Order director fluctuations in a nematic liquid crystal confined to cylindrical cavity are studied within the framework of the Frank elastic theory. In particular, eigenmodes of director fluctuations around the planar radial structure, characterized by a disclination line along the symmetry axis of the cylinder, are analyzed for $K_{11}\neq K_{22}\neq K_{33}$. The disclination line is modeled by a concentric cylindrical core; its relevant properties are described by radius, anchoring strength, and surface rotational viscosity. The eigenmodes turn out to have a peculiar phase-shifted geometrical character. The main features of the spectrum of fluctuations' eigenmodes, typical for the spectra of coupled excitations, are determined by the radial symmetry of the structure. The results of an eigenmode-based stability analysis with respect to the escape in the axial direction are in qualitative agreement with the phase diagram, obtained by comparison of the free energies of the planar and escaped radial structures. [S1063-651X(96)07508-3]

PACS number(s): 61.30.Cz, 61.30.Jf

I. INTRODUCTION

In bulk liquid crystals, the eigenmodes of order director fluctuations have been discussed quite thoroughly years ago [1]. The problem has been studied in detail in planar geometry both theoretically and experimentally, where nuclear magnetic resonance and various optical techniques are particularly important [2–8], but attempts to analyze this collective phenomenon in curved geometries are only recent [9–12].

The main aim of the study is to broaden the understanding of the dynamics of director fluctuations in the presence of the disclination line. The paper focuses on cylindrical geometry with homeotropic boundary conditions, dealing in particular with two problems: first, to determine the eigenmodes of order director fluctuations in a planar radial structure for $K_{11}\neq K_{22}\neq K_{33}$ and their spectrum, and, second, to model the coupling of the disclination line and the director fluctuations.

Linear theory of order director fluctuations in the cylindrical cavity with a planar radial director field is set up within the framework of Frank theory of liquid crystalline elasticity. The core of the disclination line is represented by a concentric cylinder, characterized by radius, anchoring strength, and surface rotational viscosity [9,13,14]. In order to reduce the number of parameters of the model and to simplify the analysis, the outer, solid boundary is assumed to impose strong homeotropic anchoring and hydrodynamic degrees of freedom are neglected.

In the next section relevant principles of nematodynamics are summarized and the analytical part of the eigenmode analysis is described. The general features of the eigenmodes' spectrum are presented in Sec. III. In Sec. IV the stability limit of the planar radial structure is discussed. The results of the study are recapitulated in Sec. V.

II. DIRECTOR DYNAMICS

A. Principles

A complete macroscopic description of a liquid crystalline state should incorporate both velocity and director field. However, the characteristic time scale of the velocity field is much shorter than the typical time of reorientation of the director field. As shown by de Gennes and Prost [15], their ratio $K\rho/\eta^2$ (K is the elastic constant, ρ the density, and η the rotational viscosity of the nematic liquid crystal) is of the order 0.01. Therefore the velocity field can be adiabatically eliminated from the dynamics of a liquid crystalline system, its influence being taken into account by a rescaled rotational viscosity.

In this approximation, the evolution of a nematic director field in the bulk is governed by the Landau-Khalatnikov-type diffusion law [15]

$$\eta\frac{\partial\mathbf{n}(\mathbf{r},t)}{\partial t}=\mathbf{h}(\mathbf{r},t), \tag{1}$$

where η is the rotational viscosity and $\mathbf{h}(\mathbf{r},t)$ is the molecular field, defined as a sum of splay, twist, and bend parts

$$\mathbf{h}=K_{11}\boldsymbol{\nabla}(\boldsymbol{\nabla}\cdot\mathbf{n})-K_{22}[A\boldsymbol{\nabla}\times\mathbf{n}+\boldsymbol{\nabla}\times(A\mathbf{n})]$$
$$+K_{33}[\mathbf{B}\times(\boldsymbol{\nabla}\times\mathbf{n})+\boldsymbol{\nabla}\times(\mathbf{n}\times\mathbf{B})]. \tag{2}$$

Following de Gennes and Prost [15], $A=\mathbf{n}\cdot(\boldsymbol{\nabla}\times\mathbf{n})$ and $\mathbf{B}=\mathbf{n}\times(\boldsymbol{\nabla}\times\mathbf{n})$; $\mathbf{h}=\mathbf{h}(\mathbf{r},t)$ and $\mathbf{n}=\mathbf{n}(\mathbf{r},t)$. The divergence terms are not taken into account, i.e., $K_{13}=K_{24}=0$.

Since the equilibrium configuration is determined by the condition $\mathbf{n}_0(\mathbf{r})\|\mathbf{h}_0(\mathbf{r})$, the above equations define the molecular field only within an additive Lagrange multiplier $\mu(\mathbf{r},t)\mathbf{n}(\mathbf{r},t)$. But since the nematic director is a unit vector, its temporal evolution is limited to rotation, i.e., $\partial\mathbf{n}/\partial t\perp\mathbf{n}$. This restriction implies that

$$\mu(\mathbf{r},t)=-\mathbf{h}(\mathbf{r},t)\cdot\mathbf{n}(\mathbf{r},t). \tag{3}$$

Similarly, the orientation of the nematic liquid crystal at the boundary ($\mathbf{n}_S$) changes according to

$$\eta_S\frac{\partial\mathbf{n}_S(\mathbf{r},t)}{\partial t}=\mathbf{g}(\mathbf{r},t), \tag{4}$$

where η_S is the surface rotational viscosity and $\mathbf{g}(\mathbf{r},t)$ is the surface molecular field [16]. Now the surface molecular field depends on both elastic torques and the interaction between the liquid crystal and the confining material G (which depends on the angle between $\mathbf{n}_S$ and an easy axis $\boldsymbol{l}$)

$$\mathbf{g}=K_{11}\mathbf{k}(\boldsymbol{\nabla}\cdot\mathbf{n}_S)-K_{22}\mathbf{k}\times(A_S\mathbf{n}_S)+K_{33}\mathbf{k}\times(\mathbf{n}_S\times\mathbf{B}_S)+\mathbf{g}_{NI}, \tag{5}$$

where $\mathbf{k}$ is the normal of the boundary, $A_S=\mathbf{n}_S\cdot(\boldsymbol{\nabla}\times\mathbf{n}_S)$, $\mathbf{B}_S=\mathbf{n}_S\times(\boldsymbol{\nabla}\times\mathbf{n}_S)$, $\mathbf{g}=\mathbf{g}(\mathbf{r},t)$, $\mathbf{n}_S=\mathbf{n}_S(\mathbf{r},t)$, and

$$\mathbf{g}_{NI}=\frac{\partial G(\mathbf{n}_S;\boldsymbol{l})}{\partial\mathbf{n}_S}. \tag{6}$$

For example, if the anchoring is homeotropic ($\boldsymbol{l}=\mathbf{k}$) and if the anchoring free energy is of the Rapini-Papoular form $[G(\mathbf{n}_S;\mathbf{k})=\frac{1}{2}W(\mathbf{n}\times\mathbf{k})^2$, where W is the anchoring strength],

$$\mathbf{g}_{NI}=W\mathbf{k}\times(\mathbf{n}_S\times\mathbf{k}). \tag{7}$$

Again, Eq. (5) defines the surface molecular field only within the transformation $\mathbf{g}(\mathbf{r},t)\rightarrow\mathbf{g}(\mathbf{r},t)+\mu'(\mathbf{r},t)\mathbf{n}_X(\mathbf{r},t)$, where $\mu'(\mathbf{r},t)$ is fixed by the condition $\partial\mathbf{n}_S/\partial t\perp\mathbf{n}_S$.

B. Eigenmodes of order director fluctuations

The planar radial structure is the simplest equilibrium nematic configuration in cylindrical geometry with homeotropic boundary conditions. Using cylindrical coordinates, its director field is described by

$$\mathbf{n}_0=\mathbf{e}_r \tag{8}$$

if $\mathbf{e}_z$ coincides with the symmetry axis of the cylinder. In the center of the capillary there is a disclination line with isotropic (or, more precisely, biaxial [17]) phase, which is energetically more favorable than the nematic phase with a diverging splay free energy density [13]. Up to linear terms, the perturbed director field is given by

$$\mathbf{n}(\mathbf{r},t)=\mathbf{n}_0+\boldsymbol{\delta}(\mathbf{r},t)=\mathbf{e}_r+P(\mathbf{r},t)\mathbf{e}_\varphi+A(\mathbf{r},t)\mathbf{e}_z, \tag{9}$$

where $P(\mathbf{r},t)$ and $A(\mathbf{r},t)$ $[P(\mathbf{r},t),A(\mathbf{r},t)\ll1]$ are planar and axial component of the director, respectively.

According to the preceding subsection, in the bulk

$$\eta\frac{\partial}{\partial t}\begin{bmatrix}1\\P\\A\end{bmatrix}=\begin{bmatrix}0\\\left(K_{33}\dfrac{\partial^2}{\partial r^2}+\dfrac{K_{33}}{r}\dfrac{\partial}{\partial r}+\dfrac{K_{11}-K_{33}}{r^2}+\dfrac{K_{11}}{r^2}\dfrac{\partial^2}{\partial\varphi^2}+K_{22}\dfrac{\partial^2}{\partial z^2}\right)P+\dfrac{K_{11}-K_{22}}{r}\dfrac{\partial^2}{\partial\varphi\partial z}A\\\left(K_{33}\dfrac{\partial^2}{\partial r^2}+\dfrac{K_{33}}{r}\dfrac{\partial}{\partial r}+\dfrac{K_{11}}{r^2}+\dfrac{K_{22}}{r^2}\dfrac{\partial^2}{\partial\varphi^2}+K_{11}\dfrac{\partial^2}{\partial z^2}\right)A+\dfrac{K_{11}-K_{22}}{r}\dfrac{\partial^2}{\partial\varphi\partial z}P\end{bmatrix}, \tag{10}$$

where $P=P(\mathbf{r},t)$ and $A=A(\mathbf{r},t)$. If K_{11}, K_{22}, and K_{33} are equal, the equation reduces to the one obtained using one elastic constant approximation [11], as it should.

The boundary conditions depend on the type of anchoring. In order to reduce the number of parameters of the model, the wall of the capillary, located at $r=R$, is assumed to induce strong homeotropic anchoring. Therefore

$$P(r=R)=A(r=R)=0. \tag{11}$$

For an isotropic Rapini-Papoular model of homeotropic anchoring, the boundary condition at the cylindrical surface of the core of the disclination with $r=r_0$ turns out to be

$$\eta_S\frac{\partial}{\partial t}\begin{bmatrix}1\\P\\A\end{bmatrix}=\begin{bmatrix}0\\\left(W+\dfrac{K_{11}-K_{33}}{r}-K_{33}\dfrac{\partial}{\partial r}\right)P\\\left(W+\dfrac{K_{11}}{r}-K_{33}\dfrac{\partial}{\partial r}\right)A\end{bmatrix}. \tag{12}$$

For a solid boundary, the anchoring strengths W usually do not exceed 10^{-5} J/m^2 [18]; for a nematic-isotropic interface, W is likely to be much smaller. The terms $(K_{11}-K_{33})/r$ and K_{11}/r, which have the same functional form as the two that belong to anchoring, are typically of the order 10^{-3} J/m^2: $K_{jj}\sim10^{-11}$ N and r_0 is probably equal to few molecular lengths, say, $\sim10^{-8}$ m [20]. Thus it is reasonable to set $W=0$ for the surface of the disclination line. In the following, $W=0$ unless indicated otherwise.

According to Eqs. (10)–(12) the radial component of the director field is not affected by the fluctuations, which are restricted to the subspace spanned by $\mathbf{e}_\varphi$ and $\mathbf{e}_z$. Therefore the reduced notation $P\mathbf{e}_\varphi+A\mathbf{e}_z\equiv[P,A]$ is used in the following.

The eigenmodes of Eq. (10) are of the relaxation type $\boldsymbol{\delta}(\mathbf{r},t)=\boldsymbol{\delta}(\mathbf{r},0)\exp(-t/\tau)$. The spatial dependence of the eigenmodes is determined using the usual separation of variables. The right-hand side of Eq. (10) is essentially a modified Laplace operator, so it is natural to seek solutions of the form

$$\boldsymbol{\delta}(\mathbf{r},t)\sim\begin{bmatrix}R_P(r)\begin{Bmatrix}\cos m\varphi\\\sin m\varphi\end{Bmatrix}\begin{Bmatrix}\cos k_3z\\\sin k_3z\end{Bmatrix}\\R_A(r)\begin{Bmatrix}\cos m\varphi\\\sin m\varphi\end{Bmatrix}\begin{Bmatrix}\cos k_3z\\\sin k_3z\end{Bmatrix}\end{bmatrix}\exp(-t/\tau), \tag{13}$$

where $R_P(r)$ and $R_A(r)$ are the radial parts of the planar and axial components of an eigenmode, respectively, and m is an integer.

[If the planar and axial components of an eigenmode do not depend on φ and z, respectively, or vice versa, they are not coupled and Eq. (10) splits into two scalar equations. These cases must be treated separately; but the procedure is analogous to the one described.]

However, not all combinations of $\cos m\varphi$ and $\sin m\varphi$ for the φ dependence and $\cos k_3 z$ and $\sin k_3 z$ for the z dependence of the planar and axial components of an eigenmode are admissible. Should we separate the variables in Eq. (10), the planar and the axial component must be an even and an odd function of φ, respectively, or vice versa. The same argument applies for the dependence of these functions on z. Therefore, one of the allowed possibilities is

$$\begin{bmatrix} \pm R_{P,1}^{\pm\pm}(r)\cos m\varphi\ \cos k_3 z \\ \pm R_{A,1}^{\pm\pm}(r)\sin m\varphi\ \sin k_3 z \end{bmatrix} \exp(-t/\tau_1^{\pm\pm}), \tag{14}$$

the superscript indices indicating the sign in front of the planar and axial component, respectively. Though it may seem that the modes with the same relative sign of the planar and axial component are linearly dependent, one can easily check that the *Ansätze*

$$[-R_{P,1}^{-+}(r)\cos m\varphi\ \cos k_3 z, +R_{A,1}^{-+}(r)\sin m\varphi\ \sin k_3 z] \times \exp(-t/\tau_1^{-+}) \tag{15}$$

and

$$[+R_{P,1}^{+-}(r)\cos m\varphi\ \cos k_3 z, -R_{A,1}^{+-}(r)\sin m\varphi\ \sin k_3 z] \times \exp(-t/\tau_1^{+-}) \tag{16}$$

give different radial parts of planar and axial component of the eigenmode. Thus there are four different eigenmodes of the above type.

There are three other combinations of sines and cosines and thus twelve more eigenmodes with the same m and k_3:

$$\begin{aligned} &[\pm R_{P,2}^{\pm\pm}(r)\cos m\varphi\ \sin k_3 z, \pm R_{A,2}^{\pm\pm}(r)\sin m\varphi\ \cos k_3 z] \times \exp(-t/\tau_2^{\pm\pm}), \\ &[\pm R_{P,3}^{\pm\pm}(r)\sin m\varphi\ \cos k_3 z, \pm R_{A,3}^{\pm\pm}(r)\cos m\varphi\ \sin k_3 z] \times \exp(-t/\tau_3^{\pm\pm}), \\ &[\pm R_{P,4}^{\pm\pm}(r)\sin m\varphi\ \sin k_3 z, \pm R_{A,4}^{\pm\pm}(r)\cos m\varphi\ \cos k_3 z] \times \exp(-t/\tau_4^{\pm\pm}). \end{aligned} \tag{17}$$

An eigenmode in a section of the capillary is schematically depicted in Fig. 1. At the lowermost cross section shown in the figure, the axial component of the eigenmode is identically 0. On moving along the capillary the axial component gradually grows while the planar component decreases and vanishes at the uppermost cross section, where the axial component reaches its maximum amplitude. The nodal lines of planar (lowermost cross section) and axial component (uppermost cross section) are mutually perpendicular. In Fig. 1 only a quarter of the eigenmode is shown. The radial parts of the planar and axial components are represented only qualitatively, i.e., they do not correspond to some particular

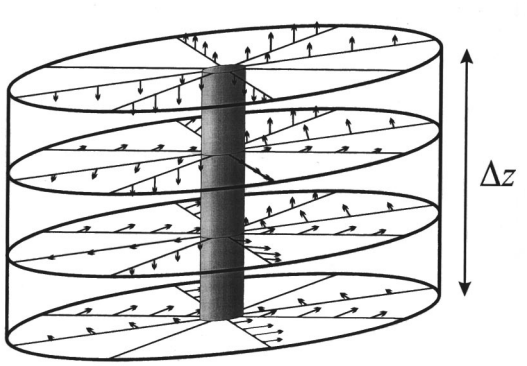

FIG. 1. Schematic representation of an eigenmode with $m=1$ and $k_s=\pi/2\Delta z$. The arrows denote the fluctuating director field and the shaded area corresponds to the disclination line. Note that the planar and axial components of an eigenmode are phase shifted with respect to φ and z.

set of elastic constants and parameters of the model of the disclination line. As indicated in the figure, the magnitudes of the two components are generally not the same. In order to ensure the completeness of the eigenmodes, periodic boundary conditions in the z direction are assumed.

The radial parts of the fluctuations' eigenmodes are determined by two coupled ordinary differential equations

$$\begin{aligned} &\left(a_3\frac{d^2}{dx^2}+\frac{a_3}{x}\frac{d}{dx}+\frac{1-a_3}{x^2}-\frac{1}{x^2}m^2-a_2\kappa^2+\lambda_i^{\pm\pm}\right)R_{P,i}^{\pm\pm} \pm\frac{1-a_2}{x}m\kappa R_{A,i}^{\pm\pm}=0, \\ &\left(a_3\frac{d^2}{dx^2}+\frac{a_3}{x}\frac{d}{dx}+\frac{1}{x^2}-\frac{a_2}{x^2}m^2-\kappa^2+\lambda_i^{\pm\pm}\right)R_{A,i}^{\pm\pm} \pm\frac{1-a_2}{x}m\kappa R_{P,i}^{\pm\pm}=0 \end{aligned} \tag{18}$$

and the boundary conditions

$$\begin{aligned} &\left((1-a_3)\frac{1}{x}-a_3\frac{d}{dx}+\alpha\lambda\right)R_{P,i}^{\pm\pm}=0, \\ &\left(\frac{1}{x}-a_3\frac{d}{dx}+\alpha\lambda\right)R_{A,i}^{\pm\pm}=0 \end{aligned} \tag{19}$$

at $x=\rho$ and

$$R_{P,i}^{\pm\pm}=0, \quad R_{A,i}^{\pm\pm}=0 \tag{20}$$

at $x=1$. In Eqs. (18)–(20) the following dimensionless variables and parameters are introduced:

$$x\equiv r/R;\ \ \rho\equiv r_0/R;\ \ \lambda_i^{\pm\pm}\equiv\eta R^2/\tau_i^{\pm\pm}K_{11},\ \ i=1,2,3,4;$$

$$a_j\equiv K_{jj}/K_{11},\ \ j=2,3;\ \ \kappa\equiv k_3 R;\ \ \alpha\equiv\eta_S/\eta R. \tag{21}$$

A brief inspection of Eqs. (18) shows that for each i there are actually only two different eigenvalues $\lambda^{\pm\pm}$ instead of four, because $R_{P,i}^{++}=R_{P,i}^{--}$, $R_{A,i}^{++}=-R_{A,i}^{--}$ on one hand and $R_{P,i}^{+-}=R_{P,i}^{-+}$, $R_{A,i}^{+-}=-R_{A,i}^{-+}$ on the other. (Equivalently, one

may choose $R^{++}_{P,i}=-R^{--}_{P,i}$, $R^{++}_{A,i}=R^{--}_{A,i}$ and $R^{+-}_{P,i}=-R^{-+}_{P,i}$, $R^{+-}_{A,i}=R^{-+}_{A,i}$.) The whole set of solutions can therefore be constructed using only two pairs of radial parts of planar and axial components of an eigenmode: one corresponds to the same and the other to the opposite signs of the coupling terms in Eqs. (18). Moreover, it is evident that the radial parts of the planar and axial components depend on the type of φ and z dependence of an eigenmode only through the signs of the coupling terms, so that the subscript indices i may be dropped. Thus the numerous collection of $R^{\pm\pm}_{P,i}$, $R^{\pm\pm}_{A,i}$, and $\lambda^{\pm\pm}_i$ can be reduced to R^{+}_{P}, R^{+}_{A}, and λ^{+}, which solve Eqs. (18) with the same sign of the coupling terms, and R^{-}_{P}, R^{-}_{A}, and λ^{-}, which represent the solution in the case of opposite signs of the coupling terms. The coupled ordinary differential equations [Eqs. (18)–(20)] are solved numerically using a standard relaxation algorithm [19].

Generally, the eigenmodes cannot be divided into those that do not contribute to splay and twist free energy, respectively, as in a bulk nematic liquid crystal [15] and in a radial nematic droplet [12]. The only exceptions are simple eigenmodes of the form

$$\left[R_P(x)\begin{Bmatrix}\cos k_3 z\\ \sin k_3 z\end{Bmatrix},0\right],\quad \left[0,R_A(x)\begin{Bmatrix}\cos m\varphi\\ \sin m\varphi\end{Bmatrix}\right],$$

with

$$\nabla\cdot\boldsymbol{\delta}=0$$

and

$$\left[R_P(x)\begin{Bmatrix}\cos m\varphi\\ \sin m\varphi\end{Bmatrix},0\right],\quad \left[0,R_A(x)\begin{Bmatrix}\cos k_3 z\\ \sin k_3 z\end{Bmatrix}\right],$$

with $\mathbf{e}_r\cdot\nabla\times\boldsymbol{\delta}=0$. Obviously, the fluctuations' eigenmodes may be classified into those of twist-bend and splay-bend type only in certain confining geometries and not in any one.

A remark on the typical values of the parameters involved is in order: m and κ should not be too large, since this would lead to deformations with very short wavelength that can no longer be treated within the continuum model. It is not trivial to estimate $m_{\max}$, but $\kappa_{\max}$ is of the order R/d (where d is the thickness of the molecule), which usually exceeds 100.

ρ is normally less than 0.1, while $a_2>0.5$ and $a_3>1$ (on approaching a nematic-smectic transition from above, k_{22} and k_{33} diverge [20]). There is, however, little data on the surface rotational viscosity, which characterizes the dynamical behavior of a nematic surface. A report on the measurement of this quantity was published only recently [21] and only few theoretical considerations of the relevant values of η_S are available at the moment [6,7,22].

III. SPECTRUM OF EIGENMODES

This section is concerned with the spectrum of the order director fluctuations' eigenmodes; the word ''spectrum'' stands for the dependence of the eigenvalue $\lambda^{\pm}$ on the wave vectors of the modulation m and κ. As already mentioned, m is an integer and κ is, due to periodic boundary conditions, a discrete real variable: $\kappa=0,\ 2\pi R/L,\ 4\pi R/L,\ 6\pi R/L,\ \ldots\ \kappa_{\max}$, where L is the length of the cylinder. Since the length of the capillaries usually used for filling with liquid crystals may well exceed $100R$ (in the case of Anopore membranes $R=0.1$ μm and $L=60$ μm) and since $\kappa_{\max}$ is usually not less than 100, κ may be treated as a continuous variable. Therefore, the three-dimensional spectrum will be represented by slices characterized by a fixed value of m. On each slice, there are several branches $\lambda^{\pm}(\kappa;m)$ that correspond to eigenfunctions with different number of nodes of $R^{\pm}_P(x)$ and $R^{\pm}_A(x)$.

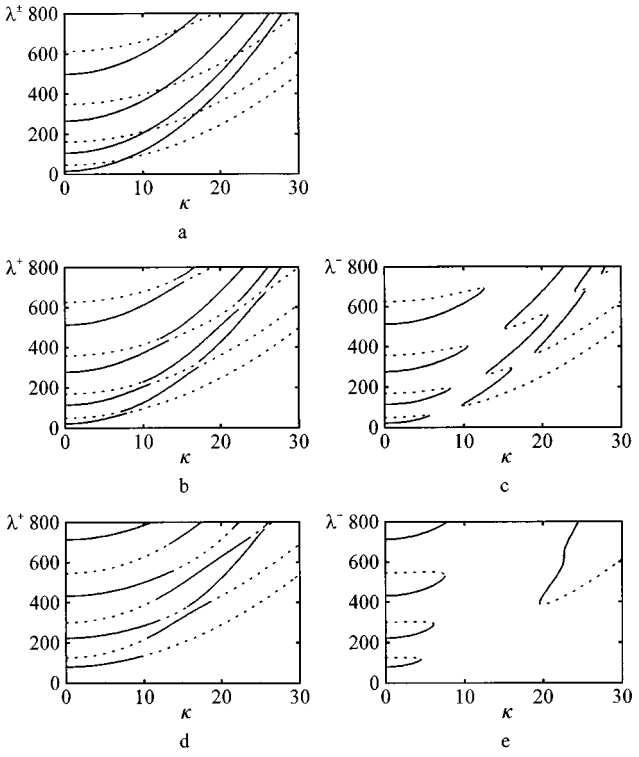

FIG. 2. Parts of the spectrum for $\alpha=0$, $a_2=0.5$, $a_3=3.5$, and $\rho=0.01$: (a) $m=0$, (b) and (c) $m=1$, and (d) and (e) $m=5$. The parts of the spectrum that correspond to the same signs of the coupling terms in Eqs. (18) [(b) and (d)] obviously evolve from the uncoupled planar and axial branches of the $m=0$ slice; the parts of the spectrum that corresponds to the opposite signs of the coupling terms [(c) and (e)] are characterized by a gap, which becomes broader and broader as m is increased. Due to the gap, the density of fluctuations' eigenmodes depends on the wave vector. (The spectrum is, of course, not limited to $\kappa<30$, $m=0$, 1, and 5, and $\lambda^{\pm}<800$.)

In Fig. 2 parts of the spectrum for $a_2=0.5$, $a_3=3.5$, $\rho=0.01$, and $\alpha=0$ are shown. For $m=0$ [Fig. 2(a)] the planar and axial components of the eigenmodes are not coupled. According to Eq. (18), the spectrum of planar modes (dotted lines) is given by $\lambda^{\pm}(\kappa)=\lambda^{\pm}(\kappa=0)+a_2\kappa^2$, while for the axial modes (solid lines) $\lambda^{\pm}(\kappa)=\lambda^{\pm}(\kappa=0)+\kappa^2$.

The situation is more interesting when $m>0$. In Fig. 2(b) the spectrum of λ^{+} is shown for $m=1$. Sections of λ^{+}'s where

$$q\equiv\frac{\max_{\rho<x<1}|R_A|}{\max_{\rho<x<1}|R_P|}\qquad(22)$$

exceeds 1 correspond to modes with a predominant axial component and are plotted with solid lines; parts of λ^{+}'s with $q<1$ represent modes of planar character and are plotted with dotted lines.

The complete slice $m=1$ is shifted upward with respect to the slice $m=0$. In addition, the eigenmodes are no longer purely planar and purely axial as for $m=0$. Roughly speaking, the coupling is strongest for values of κ that correspond to the intersections of the parabolas from Fig. 2(a), which is where the character of a solution on a particular branch λ^+ changes from planar to axial and vice versa.

Perhaps the spectrum of λ^- [Fig. 2(c)] is even more interesting. It consists of curves of two types, separated by a gap: note that the number of modes depends on κ. At small κ, the spectrum consists of hornlike curves, while for larger κ it is composed of curves that are partly sawtoothlike and partly parabolic. As in Fig. 2(b), the sections of the spectrum that correspond to planar (axial) modes are drawn with dotted (solid) line.

For larger values of m, the spectrum continues to move upward. The general features of λ^+ and λ^- remain, but, due to stronger coupling, the spectrum is more and more deformed as compared to the one with $m=1$: in Figs. 2(d) and 2(e), the spectrum for $m=5$ is shown. The trend is particularly apparent in the spectrum of λ^-, where the hornlike branches become shorter and the sawtooth curves flatten out. The gap between the two types of branches becomes broader.

The overall characteristics of the eigenmodes' spectrum turn out not to depend on boundary conditions at the inner cylinder, i.e., the radius of the disclination line, anchoring strength, and surface rotational viscosity. It is also not unreasonable to assume that they would remain the same for a different model of coupling of the nematic liquid crystal with the solid boundary. (Of course, the stability of the planar radial structure depends on these parameters. For example, if the anchoring strength at solid boundary is decreased, the whole spectrum is shifted downward and it may not be positive definite anymore. If so, the planar configuration is unstable. In this case the director fluctuations around the planar radial structure and their spectrum are not relevant anymore.)

What do the radial parts of the eigenmodes look like? Some of them, corresponding to the same sign of the coupling terms in Eq. (18), $m=1$ and $\kappa=18.5,19.0,...,21.0$, are shown in Fig. 3. With increasing κ, the number of nodes of the radial part of the planar component changes from 2 to 1 and then to 3 and its amplitude decreases. At the same time, the radial part of the axial component increases with respect to the radial part of the planar component. Generally, the $R_P^{\pm}$'s and $R_A^{\pm}$'s are wavelike as in Fig. 3.

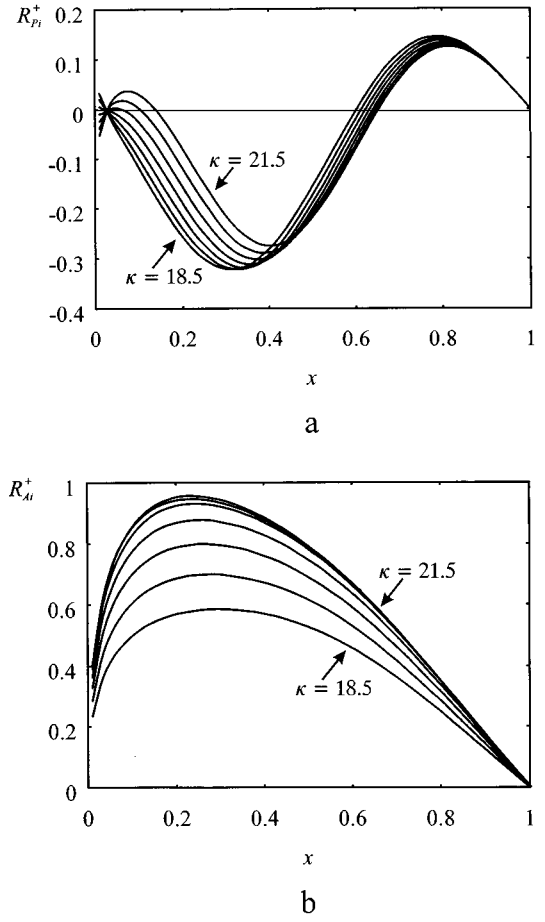

FIG. 3. Radial parts of (a) the planar and (b) the axial component of some of the eigenmodes with $\alpha=0$, $a_2=0.5$, $a_3=3.5$, $\rho=0.01$, $m=1$, and $\kappa=18.5,19.0,...,21.0$. As κ increases, the radial part of the planar component transforms from R^+_{P2} (two nodes) to R^+_{P1} (one node) and further to R^+_{P3} (three nodes). At the same time, the radial part of the axial component does not change much.

IV. STABILITY OF PLANAR RADIAL STRUCTURE

In a cylindrical capillary with strong homeotropic anchoring at the walls, the nematic liquid crystal can occur in three elementary structures: planar radial, escaped radial, and planar polar [23]. In addition to these, there are two more complex structures: escaped radial with point defects [24] and planar polar with two $s=\frac{1}{2}$ line defects [25]. The phase diagram has already been studied in detail by comparing the free energy of these structures [13,25,26].

On the other hand, one can determine the limit of stability of a structure using the eigenmode spectrum as well. The stability analysis is carried out using the positive-relaxation-rate criterion, which states that a structure is stable only if all eigenmodes of director fluctuations are damped, i.e., if all eigenvalues corresponding to the eigenmodes are positive. It is, of course, not necessary to consider the complete set of eigenvalues of the system: an analysis of the dependence of the lower limit of the spectrum on the parameters of the model is sufficient. For the planar radial structure, such an analysis has already been carried out using an analytical approach [9]. In the following, these results are verified numerically and the relevant value of the anchoring strength on the surface of the core of the disclination line is estimated.

Knowing that the lower limit of the spectrum of the eigenmodes corresponds to the modes with $m=\kappa=0$ [9], the problem is considerably simplified. In this case Eqs. (18) are not coupled: modes of this type are either purely planar $[R_A(x)=0]$ or purely axial $[R_P(x)=0]$. (Since there are no coupling terms, the superscript indices $\pm$ may be dropped.) The former must be responsible for an in-plane bend distortion of the planar radial structure and the latter should destabilize the original configuration with respect to a kind of escaped radial structure, which occurs in the same annular geometry as the planar one but exhibits an (incomplete) escape of the director field along the z axis. (It has been shown that the critical value of K_{33} for an in-plane bend distortion of the planar radial structure is lower than the threshold for

the axial bend distortion [9]: The in-plane bend distortion thus has no physical importance and it is not discussed in this paper at all.) The escapedlike radial structure is obviously not exactly equivalent to the true escaped radial configuration, but in practice the differences are not crucial for small ρ. On the other hand, it can be generated by applying a continuous transformation to the planar radial structure. Therefore, the structural transition between the two configurations is second order.

Are there any other structures that could occur in the phase diagram? If the $s=1$ disclination line, located in the center of the planar radial structure, splits into two $s=\frac{1}{2}$ lines (which are subsequently driven apart from each other by the repulsive force), the radial configuration is transformed to the planar polar structure with line defects. But the resulting director configuration is unstable unless an external field of suitable strength is applied in the direction perpendicular to the plane of the disclination lines [25]. Finally, the true planar polar structure—the director configuration with the two line defects at the confining surface—is, strictly speaking, not compatible with the concept of strong anchoring at the solid boundary. The phase diagram should therefore be divided into regions of stability of planar and escapedlike radial structure only.

The elementary axial modes in the planar radial structure are determined by

$$\left(a_3\frac{d^2}{dx^2}+\frac{a_3}{x}\frac{d}{dx}+\frac{1}{x^2}+\lambda\right)R_A=0 \tag{23}$$

and the boundary conditions

$$\left(\frac{1}{x}-a_3\frac{d}{dx}+\alpha\lambda\right)R_A=0 \tag{24}$$

at $x=\rho$ and

$$R_A=0 \tag{25}$$

at $x=1$. As it does not enter the above equations, the phase diagram obviously does not depend on a_2. On the other hand, in order to determine the stability limit of the planar radial structure one must find the values of external parameters (a_3, ρ, and α) for which the eigenvalue of the elementary axial mode vanishes. But if $\lambda=0$, the boundary condition [Eq. (24)], and therefore the solution R_A, does not depend on α, which indicates that the stability of the configuration is independent of the values of bulk and surface rotational viscosity.

In Fig. 4, the relaxation rate of the elementary axial eigenmode is shown as a function of a_3 for $\alpha=0,1,5,50$ and strong anchoring at the defect, which essentially describes the limit $\alpha\to\infty$; ρ is fixed to 0.01, a value that corresponds to submicrometer capillaries. All curves that correspond to $\alpha<\infty$ intersect the abscissa in the same point a_{3c}: planar radial structure is stable for $a_3>a_{3c}$.

As already noted, the director fluctuations destabilize the planar radial structure against the escape in the axial direction. Thus it is not unreasonable to compare the stability limits of the planar radial structure, determined (i) by the above procedure and (ii) by comparing the free energies of planar and true escaped radial configuration. In Fig. 5 the numerically obtained stability limits, calculated by method (i) for $W=0$ and $W\to\infty$ at the nematic-disclination line interface, its analytical counterparts [9], and the stability limit, obtained by method (ii) [26], are shown. The numerical results (i) are satisfactorily close to the analytical predictions and in qualitative agreement with the stability limit (ii). The quantitative discrepancy between the predictions of methods (i) and (ii) is attributed to the fact that the eigenmode-based stability analysis is carried out within the annular geometry where the true escaped radial structure does not exist: the

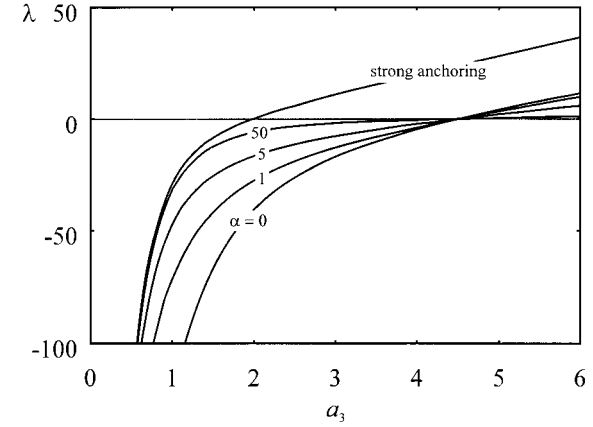

FIG. 4. Spectrum of the lowest axial eigenmode with $m=\kappa=0$, $\rho=0.01$, and completely loose anchoring at the core of the defect line ($W=0$). α, the dimensionless surface rotational viscosity, equals 0, 1, 5, and 50. The lowest part of the spectrum corresponding to strong anchoring at $x=\rho$ is also plotted.

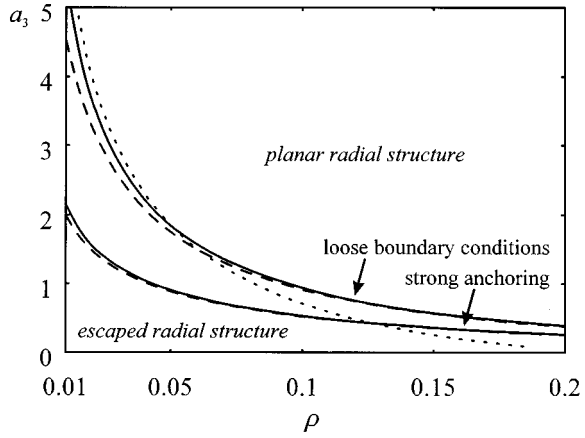

FIG. 5. Phase diagrams, corresponding to strong anchoring and completely loose boundary conditions ($W=0$) at the defect. Full line, numerically calculated stability limit, based on the eigenmode analysis; dashed line, analytical prediction [9]; dotted line, stability limit, determined by a comparison of the free energies of the planar and true escaped radial structures [26]. The escaped radial structure is stable at small a_3, while for large a_3 the planar radial configuration should be found. The numerically calculated stability limits do not depart significantly from the analytical predictions. The discrepancy between stability limits, obtained by eigenmode analysis and by a comparison of the free energies, is related to the fact that the former is carried out within the annular geometry, where the true escaped radial structure does not exist.

stability limits (i) and (ii) correspond to the transitions of the planar radial configuration to two similar yet different structures. On the other hand, this comparison indicates that whenever the nematic-disclination line interaction is modeled by a concentric cylinder as in the present study, a completely loose anchoring condition ($W=0$) at this interface is a reasonable starting point.

V. CONCLUSION

In the study, eigenmodes of order director fluctuations in planar radial structure in cylindrical capillary are analyzed within the Frank elastic theory. The core of the disclination line is modeled by a concentric cylinder, characterized by a radius, an anchoring strength, and a surface rotational viscosity. It is shown both analytically and by a stability analysis that the anchoring strength at this interface may be set to 0. The eigenmodes turned out to have a peculiar, phase-shifted geometrical character.

The spectrum of the fluctuations' eigenmodes is a typical example of dispersion of coupled excitations. The general characteristics of the spectrum of the fluctuations' eigenmodes are determined by the geometry and do not depend on details of the model of the disclination line (radius of the core of the disclination line, surface rotational viscosity, and anchoring strength): for example, the spectrum corresponding to strong anchoring at the defect is very similar to the one discussed. There is a specific feature of the spectrum of the fluctuations' eigenmodes: a gap, and therefore a reduced density of modes for certain values of m and κ. It would be interesting to see if this property of the spectrum can be checked experimentally.

The numerically obtained stability limit of the planar radial structure, obtained by the eigenmode analysis, is in good agreement with the analytical prediction. The quantitative discrepancy between the stability limits, calculated by the eigenmode analysis and by a comparison of the free energies of the planar and escaped radial structures, is related to the fact that within the present model the usual escaped configuration is approximated by an escaped structure with an isotropic cylindrical core.

The current model of the core of the defect line, based on a concept of interface characterized by an anchoring strength and a surface rotational viscosity, offers a simple and straightforward description of the nematic-disclination line interaction. However, on approaching the center of the disclination line the order parameter does not decrease discontinuously [27]. In a future work, another model of the nematic-disclination line interaction is planned to be examined, taking into account the spatial variation of the degree of order.

ACKNOWLEDGMENTS

The authors thank Professor P. Palffy-Muhoray for helpful discussions. Support from Ministry of Science and Technology of Slovenia (Grant No. J2-7067/790) and European Union (Grant No. CIPA CT-93-0159) is acknowledged.

[1] Groupe d'études des cristaux liquides (Orsay), J. Chem. Phys. **51**, 816 (1969).
[2] P. Pincus, Solid State Commun. **7**, 415 (1969).
[3] R. Blinc, D. L. Hogenboom, D. E. O'Reilly, and E. M. Peterson, Phys. Rev. Lett. **33**, 969 (1969).
[4] J. W. Doane and D. L. Johnson, Chem. Phys. Lett. **6**, 291 (1970).
[5] D. A. Dunmur and K. Szumilin, Liq. Cryst. **6**, 449 (1989).
[6] A. N. Shalaginov, Mol. Cryst. Liq. Cryst. **262**, 53 (1995).
[7] H. K. M. Vithana, G. Xu, and D. L. Johnson, Phys. Rev. E **47**, 3441 (1993).
[8] P. Galatola, C. Oldano, and M. Rajteri, Phys. Rev. E **49**, 1458 (1994).
[9] P. Palffy-Muhoray, A. Strigazzi, and A. Sparavigna, Liq. Cryst. **14**, 1143 (1993).
[10] A. D. Kiselev and V. Yu. Reshetnyak, Mol. Cryst. Liq. Cryst. **265**, 527 (1995).
[11] P. Ziherl, M. Vilfan, and S. Žumer, Phys. Rev. E **52**, 690 (1995).
[12] J. R. Kelly and P. Palffy-Muhoray (unpublished).
[13] P. E. Cladis and M. Kléman, J. Phys. (Paris) **33**, 591 (1972).
[14] P. J. Barratt, Q. J. Mech. Appl. Math. **27**, 505 (1974).
[15] P. G. de Gennes and J. Prost, *The Physics of Liquid Crystals* (Clarendon, Oxford, 1993).
[16] A. I. Derzhanski and A. G. Petrov, Acta Phys. Pol. **A55**, 747 (1979).
[17] A. Sonnet, A. Kilian, and S. Hess, Phys. Rev. E **52**, 718 (1995).
[18] L. M. Blinov, A. Yu. Kabayenkov, and A. A. Sonin, Liq. Cryst. **5**, 645 (1989).
[19] W. H. Press, B. P. Flannery, S. A. Teukolsky, and W. T. Vetterling, *Numerical Recipes* (Cambridge University Press, Cambridge, 1987).
[20] S. Chandrasekhar, *Liquid Crystals* (Cambridge University Press, Cambridge, 1992).
[21] A. G. Petrov, A. Th. Ionescu, C. Versace, and N. Scaramuzza, Liq. Cryst. **19**, 169 (1995).
[22] J. Stelzer, R. Hirning, and H. -R. Trebin, J. Appl. Phys. **74**, 6046 (1993).
[23] See, for instance, M. Vilfan and S. Žumer, Croatica Chem. Acta **65**, 327 (1992).
[24] E. Williams, P. E. Cladis, and M. Kléman, Mol. Cryst. Liq. Cryst. **21**, 355 (1973).
[25] S. Kralj and S. Žumer, Phys. Rev. E **51**, 336 (1995).
[26] R. J. Ondris-Crawford, G. P. Crawford, J. W. Doane, S. Žumer, M. Vilfan, and I. Vilfan, Phys. Rev. E **48**, 1998 (1993).
[27] H. Lin, P. Palffy-Muhoray, and M. A. Lee, Mol. Cryst. Liq. Cryst. **204**, 189 (1990).